nature medicine

Tracking the fate of glomerular epithelial cells *in vivo* using serial multiphoton imaging in new mouse models with fluorescent lineage tags

Matthias J Hackl[1–3], James L Burford[1,2], Karie Villanueva[1,2], Lisa Lam[1,2], Katalin Suszták[4], Bernhard Schermer[3], Thomas Benzing[3] & János Peti-Peterdi[1,2]

Podocytes are critical in the maintenance of a healthy glomerular filter; however, they have been difficult to study in the intact kidney because of technical limitations. Here we report the development of serial multiphoton microscopy (MPM) of the same glomeruli over several days to visualize the motility of podocytes and parietal epithelial cells (PECs) *in vivo*. In podocin-GFP mice, podocytes formed sporadic multicellular clusters after unilateral ureteral ligation and migrated into the parietal Bowman's capsule. The tracking of single cells in podocin-confetti mice featuring cell-specific expression of CFP, GFP, YFP or RFP revealed the simultaneous migration of multiple podocytes. In phosphoenolpyruvate carboxykinase (PEPCK)-GFP mice, serial MPM found PEC-to-podocyte migration and nanotubule connections. Our data support a highly dynamic rather than a static nature of the glomerular environment and cellular composition. Future application of this new approach should advance our understanding of the mechanisms of glomerular injury and regeneration.

Podocytes are critical elements of the glomerular filtration barrier (GFB), which is a complex vascular unit in the glomerular capillaries that performs plasma ultrafiltration[1]. Podocytes are highly differentiated cells that form long primary and secondary extensions that wrap around the outside of the capillary loops. Between their interdigitating foot processes, the slit diaphragm is formed, which is a key component of the GFB[2]. Recent genetic and cell biological studies have highlighted the importance of podocytes in the development of glomerular diseases[3–11]. Still, a barrier to understanding the mechanistic details of glomerular pathology is the technical limitation in studying the GFB in its native environment. Because of the lack of *in vivo* data, there are still substantial gaps in our understanding of podocyte dynamics and motility and their link to albuminuria and glomerulosclerosis. However, these insights are needed for the development of new treatment strategies.

Because of the dynamic and complex structure of the GFB, the application of high-resolution imaging tools may provide *in vivo* technology for podocyte research. MPM is an innovative, minimally invasive optical sectioning technique that allows the imaging of the mouse kidney[12], including glomeruli, *in vivo*[13–15]. Mouse genetic tools permit cell-specific expression of multicolor fluorescent proteins[16,17], including in podocytes for imaging applications[18–22]. In addition, genetic tagging and lineage tracing are powerful tools to study cell fate *in vivo*. We therefore aimed to develop a new visual approach to directly visualize and track the two glomerular epithelial cell types, podocytes and PECs, *in vivo* in the intact mouse kidney using serial MPM over time.

The motility of podocytes and PECs and their role in renal pathologies and nephron regeneration remain under debate. According to the classic view, podocytes are terminally differentiated cells and cannot repair themselves by means of cell division[23,24]. However, podocytes can proliferate in a limited number of conditions[25]. The new research field of renal stem cells has also recently challenged the stationary podocyte concept in reports that podocytes can be replaced by PECs, which migrate along the Bowman's capsule[26] and express progenitor cell markers[27]. Visual techniques to track podocytes and PECs *in vivo* may aid research on these topics and the future development of new progenitor or stem cell–based therapeutic approaches to renal injury. To test the utility of our new MPM imaging approach, we used two disease models: unilateral ureteral ligation (UUO) and Adriamycin nephropathy. UUO is a widely used animal model for studying progressive renal disease and tubulointerstitial fibrosis[28]. UUO pathology features injury of PECs and damage of the tubuloglomerular junction, leading to the formation of atubular glomeruli[29]. The rapid remodeling of the Bowman's capsule that is observed after UUO[29] suggests that this model may be ideally suited to image PEC and podocyte motility in kidney injury. Adriamycin nephropathy is a model that resembles human focal segmental glomerulosclerosis[30].

RESULTS

Characterization of podocin-GFP mice

We previously visualized podocytes on the basis of their typical position and shape by a negative labeling technique in wild-type animals

[1]Department of Physiology and Biophysics, Zilkha Neurogenetic Institute, University of Southern California, Los Angeles, California, USA. [2]Department of Medicine, University of Southern California, Los Angeles, California, USA. [3]Department II of Internal Medicine and Center for Molecular Medicine Cologne, University of Cologne, Cologne, Germany. [4]Renal, Electrolyte and Hypertension Division, Department of Medicine, University of Pennsylvania, Philadelphia, Pennsylvania, USA. Correspondence should be addressed to J.P.-P. (petipete@usc.edu).

Received 26 July; accepted 7 October; published online 24 November 2013; doi:10.1038/nm.3405

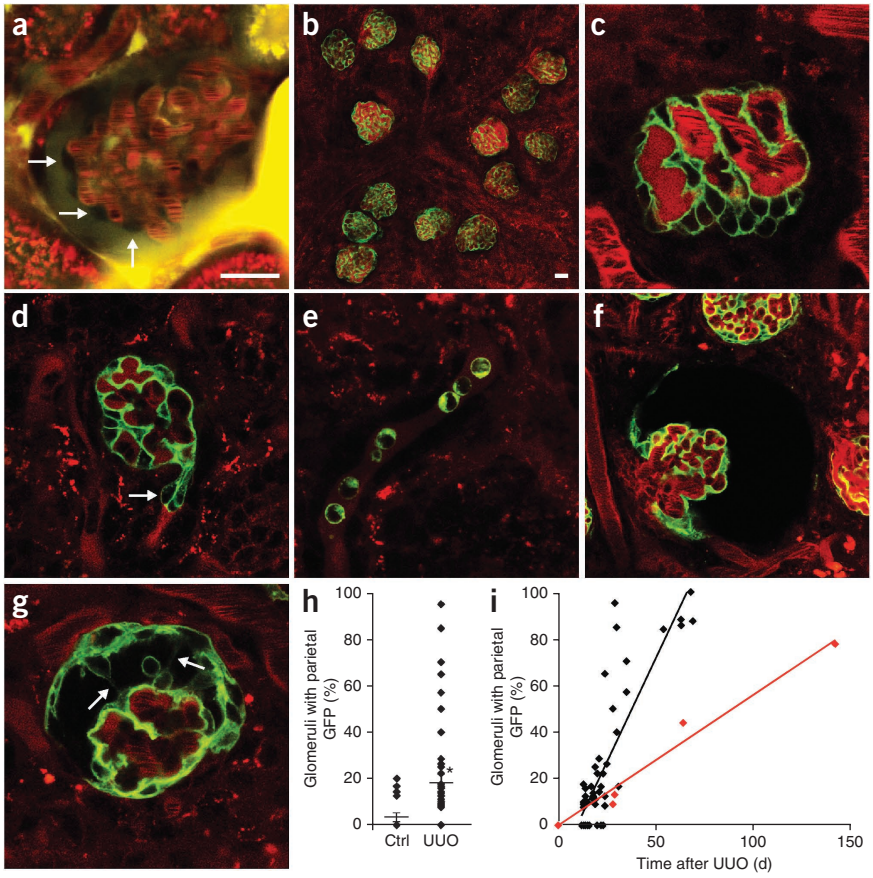

Figure 1 MPM imaging *in vivo* reveals signs of podocyte migration in the intact kidney in the model of UUO in pod-GFP mice. (**a**) In a wild-type mouse kidney, the glomerular podocytes appear as dark, unlabeled cells around capillaries (arrows). Plasma is labeled red with Alexa 594–albumin. Lucifer yellow (yellow) was injected intravenously to label the filtration (Bowman's) space. Scale bar, 20 µm (shown in **a**, applies to **a** and **c**–**g**). (**b**) Low-power image of glomeruli after UUO showing restriction of GFP fluorescence to podocytes in pod-GFP mice. Scale bar, 20 µm. (**c**,**d**) Early podocyte changes that appear after UUO include the development of podocyte cell clusters (**c**) and their projections protruding (arrow) into the lumen of the proximal tubule (**d**). (**e**) Detached, individual podocytes can be seen in the lumen of the proximal tubule. (**f**,**g**) GFP$^+$ cells in the parietal layer appear to develop by visceral podocytes migrating to the parietal layer through the vascular pole transition (**f**) or directly over the Bowman's space (**g**). Thin connections appear to bridge the parietal and visceral layers of the Bowman's capsule (arrows). Continuous GFP$^+$ cell coverage in the parietal layer develops later, at more than 3–4 weeks after UUO. (**h**) Percentage of glomeruli in which >50% of the parietal layer is covered by GFP$^+$ cells in age-matched control mice ($n = 19$) and mice at 2–5 weeks after UUO ($n = 43$). $^*P < 0.05$ using Student's t test. Data are shown as the mean ± s.e.m. Ctrl, control. The vertical dot plot shows the percentage values for each mouse. (**i**) Linear fit of the data points (black, pod-GFP ($n = 48$ mice); red, ipod-GFP ($n = 5$ mice)) showing the percentage of glomeruli with >50% parietal GFP$^+$ cell coverage. The scatter dot plot shows the percentage values for each mouse.

(mice and rats) using systemic injections of Lucifer yellow, which is a freely filterable dye[14] (**Supplementary Fig. 1a**). However, this approach precluded tracking podocytes during damage, migration or replacement. Therefore we generated a podocin-GFP (pod-GFP) mouse model in which podocytes express membrane-targeted GFP, whereas all other cells express the RFP Tomato (**Supplementary Fig. 1b**). GFP fluorescence outlined a single cell layer and was most intense close around the capillary loops as compared to the cell body because of the membrane-rich foot process region (**Supplementary Fig. 1b**). GFP-expressing podocytes colocalized with cells identified by the negative labeling technique, confirming the validity of our previous technique (**Supplementary Fig. 1c** and **Supplementary Movie 1**). Co-staining for GFP and synaptopodin, a podocyte differentiation marker, confirmed podocyte-specific expression of GFP (**Supplementary Fig. 1d**–**f**).

MPM imaging of podocyte migration

Compared to the lack of labeling in control wild-type mice (**Fig. 1a**), we observed podocyte-specific GFP expression in pod-GFP mice in a low-power MPM image of a kidney 3 weeks after UUO (**Fig. 1b**). Starting 1–2 weeks after UUO, MPM imaging visualized podocytes that formed sporadic multicellular clusters on the glomerular tuft (**Fig. 1c**), with short projections developing toward the Bowman's space and into the remainder of the proximal tubule fragment (**Fig. 1d**). We occasionally found detached single podocytes further downstream in the lumen of proximal tubules in a few filtering nephrons, indicating podocyte shedding from these projections (**Fig. 1e**). However, the most common morphological change in the UUO model was the appearance of podocytes in the parietal layer of the Bowman's capsule. In most glomeruli, podocyte projections propagated to the PEC layer after contact between podocytes and PECs was established. These contact points developed either through continuous transition at the vascular pole (**Fig. 1f**) or by forming bridges across the Bowman's space close to the urinary pole (**Supplementary Fig. 2a** and **Supplementary Movie 2**) or anywhere around the glomerular tuft (**Fig. 1g**). The podocyte projections appeared to grow further along the PEC layer toward the remodeled (sealed) glomerulotubular junction and, in some glomeruli, to the proximal tubule fragment (**Supplementary Fig. 2a**–**c**). Three to four weeks after UUO, we found a continuous layer of GFP-expressing (GFP$^+$) cells along the parietal Bowman's capsule, and numerous cell bridges of podocyte origin formed between the visceral and parietal cell layers (**Fig. 1g**). Statistical analysis (**Fig. 1h**) showed that <5 weeks after UUO, the percentage of glomeruli in which >50% of the parietal layer was covered by GFP$^+$ cells was 19 ± 4% (a total of $n = 895$ glomeruli analyzed from $n = 43$ mice; mean ± s.e.m.) compared to 3 ± 2% in age-matched control mice ($n = 239$ glomeruli from $n = 19$ mice, $P < 0.05$). The percentage of glomeruli with >50% parietal GFP$^+$ cell coverage increased continuously with time after UUO (**Fig. 1i**) ($R = 0.846$, $n = 48$ mice, $P < 0.05$). We also observed the rare phenomenon of GFP$^+$ cell projections along the parietal layer of Bowman's capsule in control healthy (non-UUO) kidneys (**Supplementary Fig. 2b**). Notably, we never observed solitary or isolated clusters of GFP$^+$ cells in the parietal layer. These cells always had continuous physical

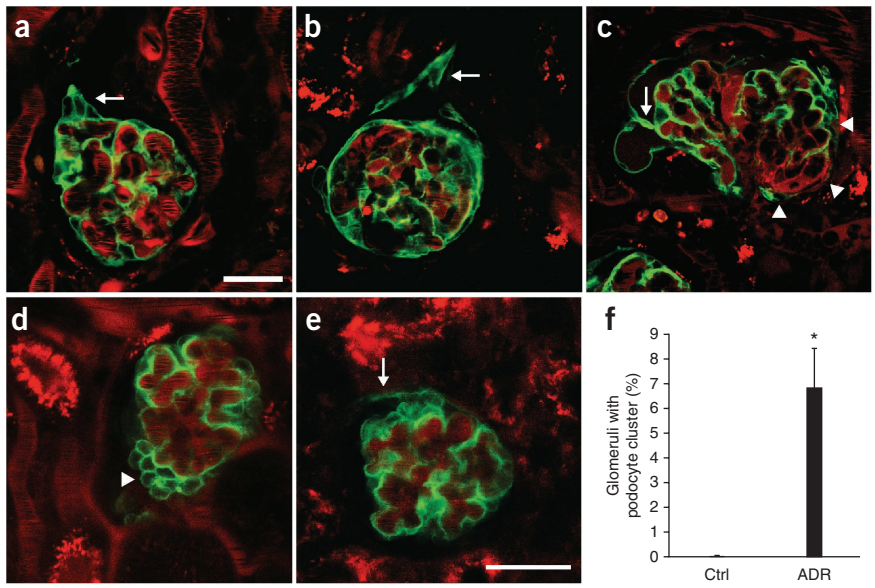

Figure 2 Confirmation of the presence of podocyte clustering and migration in ipod-GFP mice and in Adriamycin nephropathy. (**a**–**c**) Podocyte clustering and migration in ipod-GFP mice after UUO. (**d**–**f**) Podocyte clustering in the model of Adriamycin nephropathy in pod-GFP mice. In ipod-GFP mice, podocyte clustering was observed <2 weeks after UUO (**a**, arrow). At >4 weeks after UUO, podocyte projections to the parietal Bowman's capsule developed at the urinary pole invading the glomerulotubular junction (**b**, arrow), at the vascular pole transition (**c**, arrowheads) or anywhere in between the poles (**c**, arrow), giving rise to parietal GFP$^+$ cells. Plasma was labeled red with Alexa 594–albumin. MPM imaging of the intact pod-GFP mouse kidney after Adriamycin treatment revealed the presence of podocyte clusters around capillaries (**d**, arrowhead) and the development of GFP$^+$ cell coverage in the parietal layer, which was continuous with the podocyte clusters through the vascular pole transition (**e**, arrow). Scale bars, 20 µm (the bars in **a** and **e** are identical and apply to **a**–**e**). (**f**) Summary of the histological analysis showing the percentage of glomeruli with podocyte clusters in age-matched control mice and mice at 4 d after Adriamycin (ADR) treatment ($n = 4$ per group). *$P < 0.05$ using Student's t test. Data are shown as the mean ± s.e.m.

connections to the glomerular tuft, suggesting that they originated from propagating visceral podocytes. Immunolabeling of GFP and the podocyte marker podocin at 9 weeks after UUO revealed expression of podocin in GFP$^+$ cells in the PEC layer, further suggesting the migration of podocytes in this model (**Supplementary Fig. 2d**–**f**).

To confirm that GFP$^+$ cells in the parietal layer developed by migration of visceral podocytes rather than podocin gene activation in PECs (and hence, Cre-mediated GFP expression), we repeated the experiment with tamoxifen-inducible pod-GFP (ipod-GFP) mice. There was no GFP expression outside the visceral podocyte layer in ipod-GFP mice after tamoxifen induction (**Figs. 1i** and **2a**). However, at 2–4 weeks after UUO, ipod-GFP mice developed the same glomerular phenotype as described above for the constitutive pod-GFP model, including podocyte clustering (**Fig. 2a**), the development of visceral-to-parietal podocyte projections (bridging) and podocyte migration to the parietal layer (**Fig. 2b**,**c**). Statistical analysis (**Fig. 1i**) showed that similarly to the constitutive pod-GFP model, the percentage of glomeruli with >50% parietal GFP$^+$ cell coverage in ipod-GFP mice increased continuously with aging after UUO ($R = 0.972$, $n = 296$ glomeruli analyzed from $n = 5$ mice, $P < 0.05$), although the phenomenon had apparently different dynamics in the two models.

In addition, to study the effects of a different injury, we treated pod-GFP mice with a single high dose of Adriamycin. Similarly to the UUO model, within 4 d, Adriamycin treatment induced the development of sporadic podocyte clusters (**Fig. 2d** and **Supplementary Movie 3**) and the appearance of GFP$^+$ cells in the parietal layer close to the vascular pole transition and in continuum with visceral podocyte clusters (**Fig. 2e**). Histological analysis (**Fig. 2f**) revealed a significantly higher percentage of glomeruli with podocyte clusters 4 d after Adriamycin treatment (7 ± 2% from a total of $n = 1,241$ glomeruli analyzed from $n = 4$ mice) compared to 0 ± 0% in age-matched control mice ($n = 1,460$ glomeruli in $n = 4$ mice, $P < 0.05$). We measured albuminuria in the same groups and confirmed that glomerular damage developed after Adriamycin treatment (**Supplementary Fig. 3**).

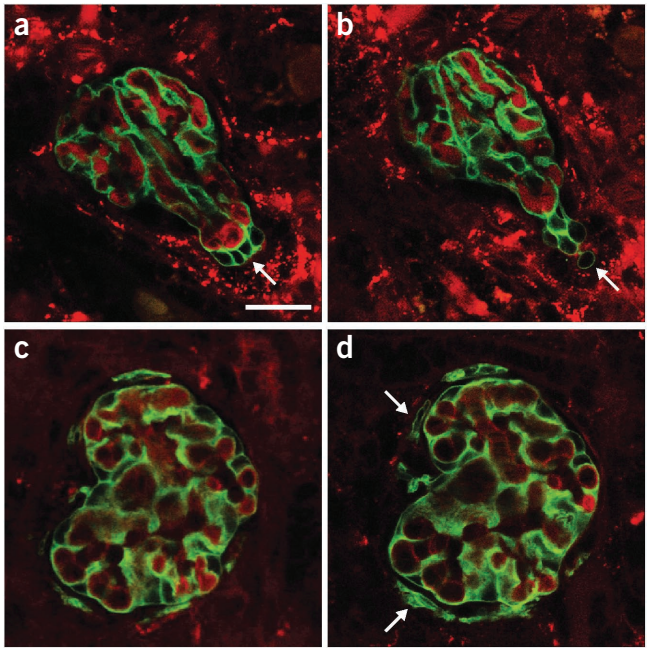

Serial *in vivo* MPM imaging of the same glomerulus

To better understand the dynamics of podocyte migration, we developed serial MPM imaging of the same glomerulus over time in the intact pod-GFP mouse kidney *in vivo* taken once every 24 h. We identified glomeruli on the basis of a laser-induced mark placed close

Figure 3 Serial *in vivo* MPM imaging of the same glomerulus in pod-GFP mice after UUO over time taken once every 24 h. (**a**,**b**) Podocytes from a hypercellular area at the urinary pole of a collapsed, nonfiltering glomerulus (**a**, arrow) appear to migrate away from the capillary tuft to form a projection into the remainder of the proximal tubule (**b**, arrow; 24 h later). (**c**,**d**) Demonstration of the increased size (growth) of the GFP$^+$ cell projections in the parietal layer (**d**, arrows) 24 h after the previous imaging session (**c**). Plasma is labeled red with Alexa 594–albumin. Scale bar, 20 µm (shown in **a**, applies to **a**–**d**).

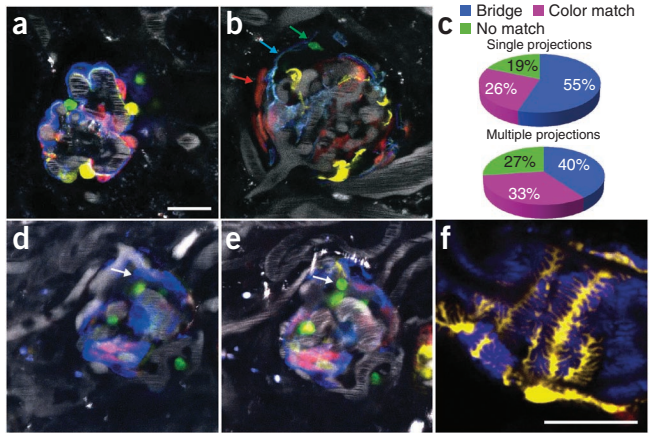

Figure 4 Identification and tracking of single podocytes in the multicolor pod-confetti mouse model using *in vivo* MPM imaging. (**a**) Podocytes are labeled in one of four colors using membrane-targeted CFP, nuclear GFP, cytosolic YFP or cytosolic RFP. Labeled dextran (plasma dye) is shown in grayscale. Scale bar, 20 µm (shown in **a**, applies to **a**, **b**, **d** and **e**). (**b**) A CFP-labeled (blue) visceral podocyte is shown bridging over the Bowman's space to the parietal layer and in direct contact with other parietal cells of the same color (blue arrow). Other adjacent parietal confetti-positive cells are labeled with RFP (red arrow) or GFP (green arrow). (**c**) Analysis of the confetti-positive cell projections between the visceral and parietal layers shown for both single, isolated projections and multiple projections in which parietal confetti-positive cells had direct contact with other projections ($n = 167$ single projections and $n = 217$ multiple projections from 112 glomeruli in 4 mice). (**d**,**e**) Serial MPM imaging of the same glomerulus showing the appearance of a nuclear GFP-labeled podocyte around a glomerular capillary (**e**) compared to 24 h earlier (**d**). Arrows indicate the same glomerular tuft region. Projection images of eight different confocal *z* planes are shown in both **d** and **e**. (**f**) Cell morphology of podocytes, including the interdigitating foot processes between two adjacent CFP- and YFP-labeled podocytes, visualized in detail (using a fixed and frozen tissue section). Scale bar, 2 µm.

to the glomerulus. We performed *z* sectioning at each time point and then compared the *z* stacks.

Serial MPM imaging was instrumental in depicting the dynamics and the substantial changes in the morphology of podocyte projections, which often occurred within 24 h of the previous imaging session. We found evidence for the migration of podocytes away from the multicellular clusters, for example, around the urinary pole into the remainder of the proximal tubule (**Fig. 3a**,**b** and **Supplementary Movie 4**). In addition, the growth of GFP$^+$ cell projections in the parietal layer was evident by the increasing length and width of the projections (**Fig. 3c**,**d** and **Supplementary Movie 5**). In the few nephrons that retained residual glomerular filtration, we observed shedding of podocytes into the proximal tubule (**Supplementary Fig. 4**).

Tracking single podocytes in podocin-confetti mice

By using podocin-confetti (pod-confetti) mice with podocyte-specific expression of membrane-targeted CFP, nuclear GFP, cytosolic YFP or cytosolic RFP (confetti construct[17]) and *in vivo* MPM imaging, we were able to identify and track individual podocytes over time on the basis of their specific color (**Fig. 4a** and **Supplementary Movie 6**). As with pod-GFP and ipod-GFP mice, UUO induced the bridging of podocytes over the Bowman's space to the parietal layer in pod-confetti mice (**Fig. 4b**). Adjacent projections in the parietal layer were often labeled by a different color, suggesting that multiple visceral podocytes migrate to the parietal Bowman's capsule. Statistical analysis of confetti-positive projections (**Fig. 4c**) showed that the majority of the projections either had a visible, monochromatic bridge between the visceral and parietal layers or the parietal confetti-positive cell matched the color of the closest visceral podocyte (81% in isolated projections and 73% in multiple projections).

In addition, serial MPM imaging of the same glomerulus in the UUO kidney of a pod-confetti mouse (**Fig. 4d**,**e** and **Supplementary Movie 7**) provided visual evidence for the appearance of new visceral podocytes within 24 h. In addition, MPM imaging of pod-confetti mice allowed the visualization of the interdigitating podocyte foot processes (**Fig. 4f**), as has been described in other genetic approaches[18,19].

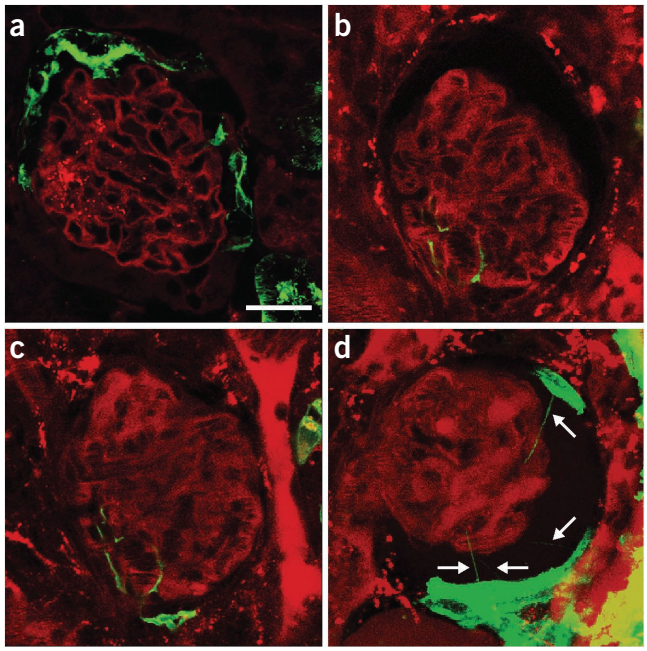

MPM imaging of PEC migration

To further elucidate the dynamic interaction between podocytes and PECs, we used *in vivo* serial MPM of PEPCK-GFP mice, which express GFP in proximal tubule segments controlled by the PEPCK promoter[31]. MPM imaging of PEPCK-GFP mouse kidneys *in vivo* revealed strong GFP expression in some, but not all, PECs in addition to in proximal tubule cells but not the glomerular tuft (**Fig. 5a**). Immunofluorescence colocalization experiments confirmed GFP expression in some PECs (**Supplementary Fig. 5**). We occasionally observed a GFP-expressing PEC at the vascular pole of the glomerulus (**Fig. 5b**,**c**), which formed projections that propagated into both the visceral and parietal layers (**Supplementary Movie 8**).

Figure 5 MPM imaging of PEC migration *in vivo* in the PEPCK-GFP mouse model after UUO. (**a**) Cell-specific GFP expression in the proximal tubule and in some, but not all, PECs. All other cells are labeled with Tomato. Scale bar, 20 µm (shown in **a**, applies to **a**–**d**). (**b**,**c**) Serial MPM imaging of the same glomerulus showing a GFP-expressing PEC at the vascular pole of the glomerulus that forms projections propagating into both the visceral and parietal layers. The length of the green projections increased between the time points 0 h (**b**) and 48 h (**c**). (**d**) Four green nanotubules (arrows) are visualized in the intact glomerulus, which appear to connect the PEC layer with the glomerular tuft.

Notably, the strong GFP expression helped visualize the presence of extremely thin nanotubules connecting PECs with the glomerular tuft after UUO (**Fig. 5d**). The width of these cell-to-cell connectors was uniform (<350 nm), and they bridged long distances between PECs and podocytes (>25 μm) across the entire Bowman's space. We also observed nanotubule connections between PECs (data not shown). The presence of PEC-to-podocyte nanotubules was common in the UUO model, with an average of one to four such nanotubules per glomerulus. Time-lapse MPM imaging revealed (**Supplementary Movie 9**) that the nanotubules were steady over time regardless of variations in hemodynamics, suggesting that these structures are indeed nanotubules rather than long primary cilia. In addition, entire cell bodies appeared occasionally along the length of the nanotubules (**Supplementary Fig. 2c**), suggesting that nanotubules may participate in podocyte migration.

DISCUSSION

Here we report the development of a new direct visual approach to track migrating podocytes and PECs over time *in vivo* in the same glomerulus of the intact kidney using serial MPM. This is an important technical advance in nephrology research to study the dynamics and interactions of different glomerular cell types in the intact glomerular environment. The tracking of cell migration and alterations in glomerular morphology may be combined with quantitative MPM imaging of key glomerular functions, as we reported recently[32–34]. The highly complex and dynamic portrayal of the structure and function of the same glomerulus during the course of a disease is one of the greatest values and advantages of this new MPM imaging technique. Accordingly, its first applications resulted in several new biological and anatomical discoveries. Serial MPM imaging provided visual evidence for podocyte motility and migration to the parietal Bowman's capsule in the intact mouse kidney *in vivo*, which were very robust after UUO. MPM imaging allowed us to visualize the development of multicellular podocyte clusters after UUO and Adriamycin treatment, as well as the highly dynamic nature of the migration of the same podocytes and PECs over several days after UUO. Moreover, a new anatomical discovery reported here is the visualization of nanotubules connecting the visceral (podocytes) and parietal (PECs) epithelial layers, which may participate in cell-to-cell communication and cell migration. The combination of serial MPM with mouse models, which allows the identification and tracking of single podocytes over time, will be very useful in future work to study mechanisms of glomerular disease and repair.

The feasibility of performing *in vivo* MPM imaging of the glomerulus in the intact mouse kidney has been demonstrated previously[13–15,34], but this is the first study, to our knowledge, that used serial MPM *in vivo* to track the fate of podocytes and PECs over time that were individually marked using fluorescent lineage tags. Serial MPM complements the powerful classical genetic cell lineage tracing tools[35] and can be combined with functional studies, for example, measurement of the glomerular permeability of macromolecules, as was recently demonstrated by our lab[32,33]. Serial MPM is a substantial new addition to the existing arsenal of tools to study podocytes and other glomerular cells[14,18,34].

MPM imaging provided important visual clues into podocyte migration that are consistent with the importance of podocyte motility and the intact actin cytoskeleton in GFB function, as has been established by a number of recent studies[3–11]. We observed signs of podocyte clustering, migration or both in not only the robust UUO model but also Adriamycin nephropathy, and even the control kidneys (although rarely), suggesting that these are general phenomena that are not restricted to UUO and may also be involved in the maintenance of the intact GFB. Serial MPM imaging over several days was instrumental in visualizing the robust dynamics of podocyte and PEC migration and remodeling. It should also be noted that protrusion and migration of these cluster cells into the proximal tubule occur in the absence of filtration, whereas podocyte detachment and shedding occur in the presence of mechanical forces. On the basis of the present findings, podocyte migration contributes to the pathological remodeling of the glomerulotubular junction and the Bowman's capsule after UUO[29]. Our data are consistent with the previously described presence of podocytes in the parietal Bowman's capsule in certain pathologies[36,37] and, rarely, the healthy kidney[38].

With longer periods of UUO, we observed a complete GFP^+ cell lining of the parietal Bowman's capsule and a progressive increase in the percentage of glomeruli with parietal GFP^+ cell coverage. These findings suggest that podocyte clustering and migration are ongoing phenomena, at least in UUO. Although mice with inducible Cre-mediated GFP expression (ipod-GFP mice) showed the same general phenotype as the constitutive pod-GFP model, further confirming podocyte migration, the parietal GFP^+ cell coverage developed faster in pod-GFP as compared to iPod-GFP mice. This effect was likely due to either imperfect Cre induction[17] in ipod-GFP mice or PEC-to-podocyte transformation in the constitutive pod-GFP mice. Also, in pod-confetti mice with constitutive Cre expression, it is possible that a change in podocyte color ('flipping') occurs even after the initial Cre recombination[39]. Therefore, the future use of inducible Cre models is required for cell lineage tracing experiments, whereas constitutive Cre reporter models may be used for short-term serial MPM imaging of cell migration.

We also found propagation of PECs in the PEPCK-GFP mouse model. We noticed Cre activity in some, but not all, PECs, as well as in the cells of the proximal tubule. Consistent with recent reports on the replacement of podocytes by PECs[26,27], serial MPM imaging was able to visualize PEC propagation into both the visceral and parietal layers at the vascular pole of the glomerulus.

The visualization of nanotubules interconnecting PECs and podocytes is an exciting anatomical discovery that was made possible by new highly fluorescent mouse models and the application of MPM *in vivo*. The (patho)physiological relevance of these physical connectors between PECs and podocytes that bridge over long distances within the Bowman's space has not yet been established. Nanotubules may provide an alternative to the vascular pole migration hypothesis that has been put forward by recent reports[26,27] and may constitute a guiding structure for cell migration directly over the Bowman's space or could be a unique form of cell-to-cell communication. Nanotubules have been reported to allow the unidirectional transfer of specific molecules and organelles between cells[40].

In conclusion, serial MPM imaging of the intact kidney *in vivo* using newly developed fluorescent lineage–tagged mouse models is a new tool to study the development of kidney disease. This imaging approach solves a critical technical barrier in podocyte research and allows the dynamic portrayal of the fate and function of various glomerular cell types *in vivo*. The results of the first applications of this technique may help change current paradigms in glomerular biology and support an emerging new concept, which emphasizes the dynamic rather than static nature of podocytes, PECs and the entire glomerular environment. Serial MPM imaging has tremendous potential and utility in the future development and testing of new regenerative therapeutic approaches.

METHODS

Methods and any associated references are available in the online version of the paper.

Note: Any Supplementary Information and Source Data files are available in the online version of the paper.

ACKNOWLEDGMENTS

This work was supported in part by US National Institutes of Health grant DK64324, American Diabetes Association grant 1-11-BS-121 and the University Kidney Research Organization to J.P.-P., Deutsche Forschungsgemeinschaft grant SFB635 to T.B. and US National Institutes of Health grant DK076077 to K.S. M.J.H. was supported by Deutsche Forschungsgemeinschaft grant HA-6212. We thank M. Hammerschmidt and H.-M. Pogoda (Institute of Developmental Biology, University of Cologne) for granting access to their imaging facility. We thank F.R. Danesh (Baylor College of Medicine) and V. Haase (Vanderbilt University) for providing podocin-iCreER^{T2} and PEPCK-Cre mice, respectively.

AUTHOR CONTRIBUTIONS

J.P.-P. conceived the study. J.P.-P., M.J.H. and J.L.B. designed the experiments, coordinated the study and analyzed the data. J.P.-P., M.J.H. and T.B. wrote the manuscript. M.J.H., J.L.B., L.L., K.V., B.S. and K.S. performed the experiments.

COMPETING FINANCIAL INTERESTS

The authors declare no competing financial interests.

1. Patrakka, J. & Tryggvason, K. New insights into the role of podocytes in proteinuria. *Nat. Rev. Nephrol.* **5**, 463–468 (2009).
2. Pavenstädt, H., Kriz, W. & Kretzler, M. Cell biology of the glomerular podocyte. *Physiol. Rev.* **83**, 253–307 (2003).
3. Boute, N. *et al. NPHS2*, encoding the glomerular protein podocin, is mutated in autosomal recessive steroid-resistant nephrotic syndrome. *Nat. Genet.* **24**, 349–354 (2000).
4. Huber, T.B. *et al.* Bigenic mouse models of focal segmental glomerulosclerosis involving pairwise interaction of CD2AP, Fyn, and synaptopodin. *J. Clin. Invest.* **116**, 1337–1345 (2006).
5. Jones, N. *et al.* Nck adaptor proteins link nephrin to the actin cytoskeleton of kidney podocytes. *Nature* **440**, 818–823 (2006).
6. Kaplan, J.M. *et al.* Mutations in ACTN4, encoding α-actinin-4, cause familial focal segmental glomerulosclerosis. *Nat. Genet.* **24**, 251–256 (2000).
7. Kestilä, M. *et al.* Positionally cloned gene for a novel glomerular protein—nephrin—is mutated in congenital nephrotic syndrome. *Mol. Cell* **1**, 575–582 (1998).
8. Mundel, P. & Reiser, J. Proteinuria: an enzymatic disease of the podocyte? *Kidney Int.* **77**, 571–580 (2010).
9. Reiser, J. *et al.* Podocyte migration during nephrotic syndrome requires a coordinated interplay between cathepsin L and α3 integrin. *J. Biol. Chem.* **279**, 34827–34832 (2004).
10. Shih, N.-Y. *et al.* Congenital nephrotic syndrome in mice lacking CD2-associated protein. *Science* **286**, 312–315 (1999).
11. Winn, M.P. *et al.* A mutation in the TRPC6 cation channel causes familial focal segmental glomerulosclerosis. *Science* **308**, 1801–1804 (2005).
12. Peti-Peterdi, J., Burford, J.L. & Hackl, M.J. The first decade of using multiphoton microscopy for high-power kidney imaging. *Am. J. Physiol. Renal Physiol.* **302**, F227–F233 (2012).
13. Devi, S. *et al.* Multiphoton imaging reveals a new leukocyte recruitment paradigm in the glomerulus. *Nat. Med.* **19**, 107–112 (2013).
14. Peti-Peterdi, J. & Sipos, A. A high-powered view of the filtration barrier. *J. Am. Soc. Nephrol.* **21**, 1835–1841 (2010).
15. Schießl, I.M., Bardehle, S. & Castrop, H. Superficial nephrons in BALB/c and C57BL/6 mice facilitate *in vivo* multiphoton microscopy of the kidney. *PLoS ONE* **8**, e52499 (2013).
16. Muzumdar, M.D., Tasic, B., Miyamichi, K., Li, L. & Luo, L. A global double-fluorescent Cre reporter mouse. *Genesis* **45**, 593–605 (2007).
17. Snippert, H.J. *et al.* Intestinal crypt homeostasis results from neutral competition between symmetrically dividing Lgr5 stem cells. *Cell* **143**, 134–144 (2010).
18. Grgic, I. *et al.* Imaging of podocyte foot processes by fluorescence microscopy. *J. Am. Soc. Nephrol.* **23**, 785–791 (2012).
19. Höhne, M. *et al.* Light microscopic visualization of podocyte ultrastructure demonstrates oscillating glomerular contractions. *Am. J. Pathol.* **182**, 332–338 (2013).
20. Khoury, C.C. *et al.* Visualizing the mouse podocyte with multiphoton microscopy. *Biochem. Biophys. Res. Commun.* **427**, 525–530 (2012).
21. Moeller, M.J., Sanden, S.K., Soofi, A., Wiggins, R.C. & Holzman, L.B. Podocyte-specific expression of cre recombinase in transgenic mice. *Genesis* **35**, 39–42 (2003).
22. Wang, J. *et al.* Tamoxifen-inducible podocyte-specific iCre recombinase transgenic mouse provides a simple approach for modulation of podocytes *in vivo*. *Genesis* **48**, 446–451 (2010).
23. Shankland, S.J. The podocyte's response to injury: role in proteinuria and glomerulosclerosis. *Kidney Int.* **69**, 2131–2147 (2006).
24. D'Agati, V.D., Kaskel, F.J. & Falk, R.J. Focal segmental glomerulosclerosis. *N. Engl. J. Med.* **365**, 2398–2411 (2011).
25. Moeller, M.J. *et al.* Podocytes populate cellular crescents in a murine model of inflammatory glomerulonephritis. *J. Am. Soc. Nephrol.* **15**, 61–67 (2004).
26. Appel, D. *et al.* Recruitment of podocytes from glomerular parietal epithelial cells. *J. Am. Soc. Nephrol.* **20**, 333–343 (2009).
27. Ronconi, E. *et al.* Regeneration of glomerular podocytes by human renal progenitors. *J. Am. Soc. Nephrol.* **20**, 322–332 (2009).
28. Chevalier, R.L., Forbes, M.S. & Thornhill, B.A. Ureteral obstruction as a model of renal interstitial fibrosis and obstructive nephropathy. *Kidney Int.* **75**, 1145–1152 (2009).
29. Forbes, M.S., Thornhill, B.A. & Chevalier, R.L. Proximal tubular injury and rapid formation of atubular glomeruli in mice with unilateral ureteral obstruction: a new look at an old model. *Am. J. Physiol. Renal Physiol.* **301**, F110–F117 (2011).
30. Dai, C., Saleem, M.A., Holzman, L.B., Mathieson, P. & Liu, Y. Hepatocyte growth factor signaling ameliorates podocyte injury and proteinuria. *Kidney Int.* **77**, 962–973 (2010).
31. Rankin, E.B., Tomaszewski, J.E. & Haase, V.H. Renal cyst development in mice with conditional inactivation of the von Hippel-Lindau tumor suppressor. *Cancer Res.* **66**, 2576–2583 (2006).
32. Nakano, D. *et al.* Multiphoton imaging of the glomerular permeability of angiotensinogen. *J. Am. Soc. Nephrol.* **23**, 1847–1856 (2012).
33. Salmon, A.H.J. *et al.* Loss of the endothelial glycocalyx links albuminuria and vascular dysfunction. *J. Am. Soc. Nephrol.* **23**, 1339–1350 (2012).
34. Kang, J.J., Toma, I., Sipos, A., McCulloch, F. & Peti-Peterdi, J. Quantitative imaging of basic functions in renal (patho)physiology. *Am. J. Physiol. Renal Physiol.* **291**, F495–F502 (2006).
35. Smeets, B. *et al.* Tracing the origin of glomerular extracapillary lesions from parietal epithelial cells. *J. Am. Soc. Nephrol.* **20**, 2604–2615 (2009).
36. Benigni, A. *et al.* Inhibiting angiotensin-converting enzyme promotes renal repair by limiting progenitor cell proliferation and restoring the glomerular architecture. *Am. J. Pathol.* **179**, 628–638 (2011).
37. Gibson, I.W., Downie, T.T., More, I.A. & Lindop, G.B. Atubular glomeruli and glomerular cysts—a possible pathway for nephron loss in the human kidney? *J. Pathol.* **179**, 421–426 (1996).
38. Bariety, J., Mandet, C., Hill, G.S. & Bruneval, P. Parietal podocytes in normal human glomeruli. *J. Am. Soc. Nephrol.* **17**, 2770–2780 (2006).
39. Schepers, A.G. *et al.* Lineage tracing reveals Lgr5^{+} stem cell activity in mouse intestinal adenomas. *Science* **337**, 730–735 (2012).
40. Rustom, A., Saffrich, R., Markovic, I., Walther, P. & Gerdes, H.-H. Nanotubular highways for intercellular organelle transport. *Science* **303**, 1007–1010 (2004).

ONLINE METHODS

Animals. Both male and female C57BL/6J mice at the age of 4–12 weeks were used randomly. Four new fluorescent reporter mouse models were generated. (i) Pod-GFP, by crossing mice expressing Cre recombinase under the control of the podocin promoter[21] and animals with a Tomato^{floxSTOP}-eGFP sequence in the ROSA 26 locus (B6.129(Cg)-*Gt(ROSA)26Sor*$^{tm4(ACTB-tdTomato,-EGFP)Luo}$)[16]. This results in expression of Tomato in all cells except podocytes, which express GFP. To study the effects of different backgrounds, the mice were used in a C57BL/6 background or a FVB background, or the F1 generation crossed between these backgrounds was used. (ii) ipod-GFP, by crossing mice expressing tamoxifen-inducible improved Cre recombinase under the control of the podocin promoter (podocin-iCreER^{T2} mice[22], kind gift from F.R. Danesh, Baylor College of Medicine) and animals with the Tomato^{floxSTOP}-eGFP construct mentioned above. (iii) PEPCK-GFP, by crossing mice expressing Cre recombinase under the control of the phosphoenolpyruvate-carboxykinase promoter (PEPCK-Cre, kind gift from V. Haase, Vanderbilt University)[31] and animals with the Tomato^{floxSTOP}-eGFP construct mentioned above. (iv) Pod-confetti, by crossing mice expressing the R26R-confetti construct[17] and podocin-Cre mice[21], resulting in the expression of membrane-targeted CFP, nuclear GFP, cytosolic YFP or cytosolic RFP in podocytes. All animals were purchased from the Jackson Laboratory (Bar Harbor, ME) unless otherwise noted. All animal protocols were approved by the Institutional Animal Care and Use Committee at the University of Southern California or by local government authorities in Germany (Landesamt für Natur, Umwelt und Verbraucherschutz Nordrhein-Westfalen) under the license 8.87-50.10.31.08.049.

Tamoxifen induction. 4-week-old mice received tamoxifen chow (40 mg per kg body weight; Harlan Laboratories, Indianapolis, IN) for 2 weeks, which was followed by a 2-week washout period before additional procedures were performed.

UUO. Between 3 and 8 weeks of age, the animals were anesthetized with isoflurane, and after a midline laparotomy, the left ureter was exposed and ligated three times. Successful ligation was confirmed by the hydronephrotic distension of the kidney at the time of imaging.

Adriamycin nephropathy. Pod-GFP animals received a single dose of 25 mg per kg body weight Adriamycin (doxorubicin) by retro-orbital injection; the animals were then imaged and sacrificed, and their tissues were collected 4–6 d later. Successful induction of albuminuria was confirmed by measuring the urinary albumin-to-creatinine ratio (Exocell, Philadelphia, PA) between days 0 and 6 after Adriamycin treatment.

Multiphoton imaging. The animals were anesthetized with a combination of ketamine (100 mg per kg body weight) and xylazine (10 mg per kg body weight). A tracheal tube was inserted to facilitate breathing, and the right carotid artery and/or jugular vein was cannulated for dye infusion. 70-kDa Texas Red dextran or Alexa 594 bovine serum albumin was injected to label the vasculature. In some experiments, Lucifer yellow (Invitrogen) was injected as an intravenous bolus to visualize glomerular filtration. The left kidney was exteriorized through a flank incision, and the animal placed on the microscope stage as described previously[34]. Body temperature was maintained with a homeothermic blanket system (Harvard Apparatus). The images were acquired using a Leica TCS SP5 multiphoton confocal fluorescence imaging system with a 63× Leica glycerine-immersion objective (numerical aperture (NA) 1.3) powered by a Chameleon Ultra-II MP laser at 860 nm (Coherent) and a DMI 6000 inverted microscope's external nondescanned detectors. Short-pass filters (680 nm for blue and red and 700 nm for green and yellow), dichroic mirrors (cut off at 515 nm for green and yellow and at 560 nm for blue and red) and bandpass filters were specific for detecting CFP, GFP, YFP and RFP emission (473, 514, 545 and 585 nm, respectively) (Chroma). The images of ipod-GFP animals were acquired using the external detectors of an inverted Zeiss LSM710 NLO multiphoton confocal fluorescence microscope powered by a Chameleon Ultra-II MP laser at 860 nm and a 40× Zeiss water-immersion objective (NA 1.2).

Serial survival imaging of the same glomerulus. After anesthesia, the left kidney was exteriorized by a small cut in the left flank below the kidney to avoid sutures right above the kidney afterwards. To avoid invasive vascular access surgeries, the dyes were administered by retro-orbital injections. The animal was transferred to the microscope stage, and the exteriorized kidney was placed into a kidney cup. An area of the kidney that was suitable for imaging was identified, and the position of the kidney was noted for identical placement on the following days. After acquiring *z* stacks of the glomerulus, a small distant area in the field of view was marked by shortly focusing the laser beam on this area with high power. This maneuver generated an easy-to-find highly fluorescent spot (reference point) that remained there for 3–5 d. The position of the mark relative to the glomerulus of interest was documented. After imaging, the kidney was placed back into the retroperitoneum, and the flank cut was closed with two layers of sutures. This procedure was repeated 24 and 48 h later by removing the sutures and exteriorizing the kidney again. With this technique, we were able to subsequently find approximately 70% of the glomeruli that were marked in the first imaging session. *Z* stacks of marked glomeruli were acquired with imaging settings identical to those used the day before.

The potential toxicity of laser excitation and fluorescence to the cells was minimized by using a low laser power and high scan speeds to keep total laser exposure as minimal as possible. The usual image acquisition consisted of only one *z* stack per glomerulus (<1 min) per 24 h, which resulted in no apparent cell injury. Serial imaging once every 24 h for up to 72 h after the first imaging session and the associated multiple, dorsal abdominal surgeries did not cause visible tissue adhesions or renal fibrosis.

***Z*-stack analysis.** *Z* stacks from different time points were aligned using StereoMovie Maker (http://stereo.jpn.org) to visualize changes over time in a side-by-side fashion (**Supplementary Movies 4**, **5**, **7** and **8**).

Immunohistochemistry. Animals were perfused with ice-cold PBS into the left ventricle followed by ice-cold 4% paraformaldehyde for 2 min each. Antigen retrieval was performed on paraffin sections with a heating step for 8 min at 95 °C in a citrate buffer using a pressure cooker. The sections were incubated with primary antibodies to the following proteins overnight (1:100 dilution unless stated otherwise): synaptopodin (mouse, clone G1D4, Progen, Heidelberg, Germany), podocin (1:250, rabbit, P0372, Sigma-Aldrich, St. Louis, MO), claudin-1 (1:250, rabbit, SAB4200462, Sigma), villin (mouse, clone 1D2C3, Immunotech, Chicago, IL), GFP (chicken, GFP-1020, Aves, Tigard, OR) and GFP (rabbit, A11122, Invitrogen) followed by incubation with the secondary antibodies conjugated with Alexa 488 or 594 (Invitrogen). Confocal fluorescence microscopy was performed using the same Leica TCS SP5 microscope as described above.

Statistical analyses. Data are expressed as the mean ± s.e.m. and were analyzed in a nonblinded fashion using Student's *t* test or linear regression (*R* value), as indicated. $P < 0.05$ was considered significant. For the statistical analyses of visceral to parietal projections in confetti-UUO mice, multiple projections were defined as projections in which parietal confetti-positive cells had direct contact with other projections ($n = 167$ isolated projections and $n = 217$ multiple projections from a total of $n = 112$ glomeruli analyzed from 4 mice).